

This is a repository copy of *A compact electron gun for time-resolved electron diffraction*.

White Rose Research Online URL for this paper:

<https://eprints.whiterose.ac.uk/93800/>

Version: Accepted Version

Article:

Robinson, Matthew S., Lane, Paul D. and Wann, Derek A. orcid.org/0000-0002-5495-274X (2015) A compact electron gun for time-resolved electron diffraction. *Review of Scientific Instruments*. 013109. ISSN 0034-6748

<https://doi.org/10.1063/1.4905335>

Reuse

Items deposited in White Rose Research Online are protected by copyright, with all rights reserved unless indicated otherwise. They may be downloaded and/or printed for private study, or other acts as permitted by national copyright laws. The publisher or other rights holders may allow further reproduction and re-use of the full text version. This is indicated by the licence information on the White Rose Research Online record for the item.

Takedown

If you consider content in White Rose Research Online to be in breach of UK law, please notify us by emailing eprints@whiterose.ac.uk including the URL of the record and the reason for the withdrawal request.

A compact electron gun for time-resolved electron diffraction

Matthew S. Robinson,¹ Paul D. Lane,^{1,2} and Derek A. Wann^{1,a)}

¹ *Department of Chemistry, University of York, Heslington, York, YO10 5DD, UK*

² *Present address: Department of Physics, University of Strathclyde, 107 Rottenrow East, Glasgow, G4 0NG, UK*

^{a)} Electronic mail: derek.wann@york.ac.uk

A novel compact time-resolved electron diffractometer has been built with the primary goal of studying the ultrafast molecular dynamics of photoexcited gas-phase molecules. Here we discuss the design of the electron gun, which is triggered by a Ti:Sapphire laser, before detailing a series of calibration experiments relating to the electron-beam properties. As a further test of the apparatus, initial diffraction patterns have been collected for thin, polycrystalline platinum samples, which have been shown to match theoretical patterns. The data collected demonstrate the focusing effects of the magnetic lens on the electron beam, and how this relates to the spatial resolution of the diffraction pattern.

I. INTRODUCTION

Since the work of Davisson and Germer in 1927¹ the interactions of electron beams with gaseous and crystalline samples have been used extensively to determine the structures of molecular species. Conventional gas electron diffraction experiments, using continuous beams of electrons, are typically conducted over timescales ranging from significant fractions of a second to many minutes or even hours. One consequence of this is that the structures determined are time averaged, with any information about dynamic structural effects being lost. Since the development of ultrafast laser sources and the subsequent application of femtochemical techniques to spectroscopy,² electron diffraction has adapted to allow studies to be performed on sub-picosecond timescales.³ This has now advanced to the point where molecular movies can be recorded, showing the evolution of molecular structures during induced chemical and physical processes.⁴

The early steps in time-resolved electron diffraction (TRED) were taken by Ischenko, who, in 1983, demonstrated a stroboscopic beam of electrons allowing molecular structures to be obtained with microsecond time resolution.⁵ These experiments involved the use of electromagnetic deflector plates to manipulate a continuous electron beam and chop it into

pulses before performing pump-probe experiments on the photodissociation of excited CF₃I molecules.⁵ In 1992 Ewbank introduced a new method of producing short bunches of electrons using a laser and a photocathode;⁶ this enabled shorter electron pulses to be obtained more easily. Much of the subsequent early work in this area was performed by Zewail, who achieved electron diffraction with a time resolution on the picosecond timescale.^{7–10} Zewail also developed important theory underpinning TRED experiments, detailing the velocity mismatch problem that exists between electron pulses and laser pulses, and proposed changes to the geometry of the beams in the interaction region to minimize velocity mismatch.¹¹ Further theoretical advances were made by Qian,^{12,13} and by Siwick,^{14,15} who debated in the literature the implications of space-charge broadening and how this limits the temporal resolution of the TRED technique. A number of methods have since been employed to obtain better temporal resolution in TRED experiments, including the application of RF cavities,^{16–18} single-electron electron diffraction,^{19,20} and electron diffraction using MeV electrons;^{21–23} the latter has the potential to allow single-shot experiments, removing the limitation of studying reversible systems.

A number of studies have been performed using TRED to look at order-disorder transitions such as the melting of aluminum,^{21,24,25} as well as order-order transitions in cyclohexadiene,²⁶ silicon,²⁷ graphite,²⁸ bismuth,²⁹ diarylethene,³⁰ and EDO-TTF.⁴ The application of TRED in reflection mode (rather than transmission mode) also allows time-resolved studies of surfaces to be performed.^{31,32} The majority of studies using TRED have involved crystalline and polycrystalline samples, with relatively few studies published for gas-phase samples beyond the early work of Zewail.³³ One notable exception is the work of Centurion,³⁴ who recently showed that it is possible to use electron pulses to obtain non-circularly-symmetric gas-phase diffraction patterns, by temporarily aligning molecules non-adiabatically with ultrafast laser pulses. Upon resolving these patterns using holographic methods, an increase in the amount of data collected is observed compared to experiments using randomly oriented samples of molecules.³⁴

The apparatus described here has been developed primarily to look at molecules in the gas phase, allowing the structures and dynamics of species to be determined in an environment where they are free from solvent interactions and packing forces. Structural information will be obtained for photoactive species with an atomic level of detail not achievable using spectroscopic techniques alone. The diffractometer produces electrons by ionizing a gold photocathode using the third harmonic ($\lambda = 267$ nm) of a Ti:Sapphire laser. The electrons are accelerated across a potential of up to 100 kV towards a grounded anode, after which they

propagate in a field-free region where they encounter a sample and are scattered, with the resulting diffraction pattern recorded using a phosphor screen / CCD detector.

II. SPACE-CHARGE EFFECTS

One of the main challenges in developing a time-resolved electron diffractometer is minimizing the effects of space-charge repulsion, a factor that has strongly influenced the design of this instrument. While the electron pulses created at the photocathode have similar properties to the laser pulses used to create them,³⁵ the negative charges mean that the electrons within the pulses repel one another causing the pulses to expand both spatially and temporally. This process starts immediately after the electron pulses leave the photocathode and continues as they propagate through the system. The rate at which the electron pulses expand depends on a number of factors including the initial pulse duration, the number of electrons in the pulse, and the group velocity of the pulse. Siwick *et. al.*¹⁴ reported that a pulse containing 10^4 electrons, accelerated across 30 keV, with an initial duration of 50 fs will have expanded to approximately 6.5 ps after propagating for 4 ns. Moreover, shorter laser pulses produce electron bunches that expand more rapidly because of the greater initial charge density.¹⁴

Using pulses containing a single electron can effectively nullify the space-charge effects,¹⁷ though implementing such an approach would vastly increase the time required to record data. Another potential tactic for avoiding space-charge repulsion involves using MeV electrons, as Columbic repulsion is far less of a problem when approaching relativistic speeds.¹⁸ However, creating MeV electrons requires the use of a linear accelerator and, while such instruments exist,¹⁸ the further development of tabletop systems is vital to enable cost-effective studies that are accessible to more researchers.

The velocity distribution of the electrons produced by a photocathode can be described as a linear chirp,¹⁴ with the electrons at the front of the pulse being accelerated by the electrons behind them, while the electrons at the rear of the pulse are decelerated by the electrons in front of them. Applying a rapidly switching radio-frequency (RF) electric field,³⁶ allows the electrons at the front of the pulse to be slowed down and the electrons at the back of the pulse to be accelerated, thus compressing the pulse in the temporal dimension as demonstrated by Miller,¹⁷ and by Siwick.¹⁸ Another approach taken by Schwoerer utilizes the space-charge repulsion to create picosecond electron pulses.³⁷ A streak camera deflects each pulse in the transverse direction enabling the observation of the entire temporal profile of the pulse at the

detector. This has the potential to allow the molecular dynamics of a sample to be recorded in a single shot rather than as a series of experiments with varying pump-probe delay times.³⁸

III. INSTRUMENT

For the TRED apparatus described here we have chosen to address the space-charge problem by designing a compact electron gun; this minimizes the distance that the electrons travel between the gun and the sample, thus limiting the degree of expansion of the pulse. Particle tracing simulations, using General Particle Tracer³⁹ and SIMION,⁴⁰ indicate that a pulse containing 10^4 electrons will have a duration of approximately 1.3 ps full width at half maximum (FWHM) at 45 kV when the sample is positioned 130 mm from the anode. At this voltage a FWHM transverse beam diameter of 0.34 mm is predicted at the sample, when using a 150 μm aperture in the anode of the electron gun. Assuming that one can set the transverse diameter of both the laser and molecular beams to a similar size (*i.e.* ~ 0.35 mm) an overall experimental time resolution of 2.5 ps is predicted at 45 kV with the experimental set-up described here, where all three beams are orthogonal to one another. Future routine experiments, carried out at 100 kV, are predicted to have pulse durations of 375 fs FWHM, and will also make use of a 150 μm aperture in the anode to produce a FWHM transverse beam diameter of 0.14 mm at the sample. Again assuming that one can produce both a laser and molecular beam with similar transverse widths (*i.e.* ~ 0.15 mm), and intersect the pump and probe beams at angle of approximately 60° , an experimental time resolution of 670 fs is predicted.⁴¹ Figure 1 shows the layout of the apparatus with the main components of the system discussed in detail below.

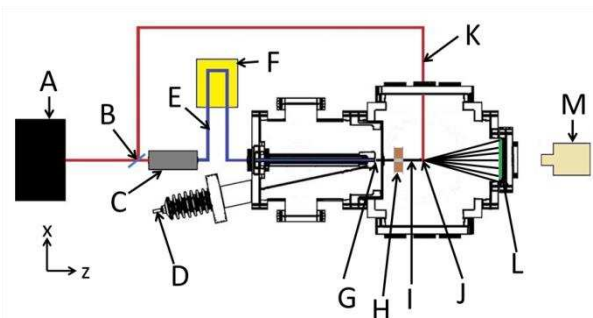


FIG. 1. A schematic diagram (not to scale) of the TRED apparatus showing A) Ti:Sapphire laser, B) 70:30 beam splitter, C) third-harmonic-generation setup, D) high-voltage feed through, E) electron ionization laser path, F) delay stage, G) photocathode, H) magnetic lens, I) electron beam, J) sample position/interaction region, K) pump laser path, L) electron detector, and M) CCD camera.

A. Optics

The laser system used for the TRED experiments consists of a Ti:Sapphire oscillator and an amplifier to produce pulses of 150 fs at a central wavelength of 800 nm (80 nm bandwidth); the repetition rate is 1 kHz and the beam power is approximately 1 W. The laser beam is then separated into two branches using a 70:30 beam splitter, with 30% of the beam being used to create the electron probe pulse and the remaining 70% used as a pump laser to excite samples. Detailed discussion of pump-probe methodologies is beyond the scope of this paper; for more information on this subject we refer the reader to Ref. 3. In order to create the electron probe pulse, the laser beam is passed through a frequency tripling system to produce pulses of 267 nm wavelength, which are then separated from the fundamental and second harmonic frequencies using dichroic mirrors. For the experiments described below, the third-harmonic beam (maximum pulse energy approximately 200 nJ) is focused onto the photocathode of the electron gun with a spot size diameter of approximately 200 μm . Small changes in the focus of the laser beam did not appear to affect the electron beam produced from the photocathode. Using an unfocused laser, however, results in almost no electrons being produced.

B. Electron gun

The TRED apparatus is designed with the electron gun housed in a differentially pumped vacuum chamber, separate from the diffraction zone. This minimizes the amount of sample gas that can enter the electron gun chamber, as that would increase the likelihood of electrical discharging. The gun chamber typically operates at a pressure of 5×10^{-8} mbar, with a titanium anode forming the boundary between this chamber and the diffraction chamber. In the center of the anode is an aperture allowing the electrons to exit the gun chamber.

The electron gun comprises of a photocathode (labelled A in Figure 2), stainless steel electrode (B), and ceramic tube (C). The photocathode is back illuminated by the 267 nm laser light, and is of similar design to the one described by Siwick.³⁵ It consists of a sapphire disc (13 mm diameter and 0.5 mm thick) coated with a 25 nm layer of gold on the front side and with a 200 nm metallic coating around the edges to provide an electrical contact with the electrode. The majority of the back of the sapphire disc is masked during preparation and remains uncoated so that the laser light can pass through the sapphire disc and reach the gold film on the front. This photocathode sits tightly in a recess on the electrode, with the front of the photocathode flush with the outer edge of the electrode to minimize discontinuities in the electric field that might lead to discharging. The electrode is mounted on a 315 mm long

ceramic tube with ribbing on the surface to maximize the surface area and reduce charge creep.⁴² The laser beam enters the chamber through a sapphire (DUV) viewport in the rear flange and passes through the inner bore of this ceramic tube to the photocathode.

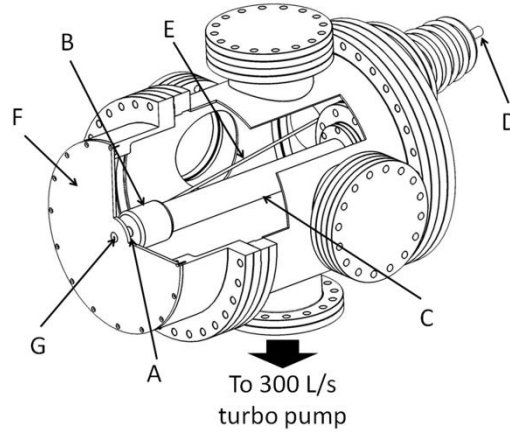


FIG. 2. A cut-through diagram of the electron-gun chamber showing A) photocathode, B) electrode, C) ceramic tube, D) high-voltage feed through, E) high-voltage pin, F) anode plate, and G) anode plug.

A potential of up to 100 kV is applied to the electrode using a high-precision Heinzinger power supply attached to the high-voltage feed through (D), with a number of precautions taken to reduce the probability of the high-voltage power supply arcing to the chamber. The high-voltage feed through enters the chamber through the rear flange of the electron gun at an angle of 12° to the axis of the ceramic tube. This keeps the bare high-voltage pin (E) as far away as possible from the grounded walls of the chamber, and prevents it from having to be bent in order to reach the electrode. The electrode itself is enclosed by a ceramic cup leaving only the photocathode exposed, again to help prevent arcing. The photocathode-to-anode distance used in the experiments described here was 17 mm, although this distance can be adjusted with the introduction of spacer plates. In the center of the anode plate (F) there is an anode plug (G) that is designed to hold various sizes of platinum apertures (of the kind typically used in electron microscopes) allowing control over the emerging electron beam. The advantage of using a smaller aperture is that a less divergent electron beam can be achieved; however, this is at the cost of a reduced number of electrons per pulse and, hence, longer data-acquisition times.

We find that using a magnetic lens to focus the electron beam allows the beam divergence to be further controlled, resulting in a narrower beam without reducing the beam current.

However, the inclusion of the lens requires greater space to be left between the photocathode and the sample, resulting in a slightly poorer temporal resolution. The system was designed in as flexible a way as possible so that all of these components can be adjusted or removed as the needs of an experiment are determined. For the initial diffraction studies reported here we use an aperture 1 mm diameter and the magnetic lens as detailed below.

C. Magnetic lens

The magnetic lens used to focus the electron beam is based on the principles of a solenoid.⁴³ The core of the lens is an iron spool, which is 20 mm long and with a 10 mm central bore through which the electron beam passes. Around the outside of the spool are approximately 1,000 turns of Kapton-coated wire, through which a current of up to 3 A can be applied. By varying the lens current the electron beam can be focused to reduce its diameter (spot size), which is desirable as the spatial resolution of an electron diffraction experiment is dependent on the spot size. For the 45 keV beam energy used for the initial diffraction study presented here we find that a current range of 1.1 to 1.3 A is sufficient to obtain a good focus at the detector, which is 330 mm from the front of the anode. Overfocusing the electron beam can create a large Coulomb-repulsion effect that causes the beam to expand rapidly in both the spatial and temporal frames, resulting in a marked loss of resolution.

The lens is mounted on an *xyz* manipulator, allowing fine control of its position with respect to the electron beam. If the beam is not passing through the center of the lens, or if the lens winding is uneven, the beam could be deflected away from its desired position at the center of the detector. A power supply stable to within 0.01 A is used as fluctuations in current can cause the electron beam to be deflected. The heat generated by the lens must be dissipated as the resistance of the wire varies with temperature and so the lens is cooled using liquid nitrogen. A copper braid connects the liquid nitrogen vessel to the lens and the temperature is monitored using thermocouples.

D. Diffraction chamber

The apparatus has been designed primarily to study gas-phase samples and the main chamber needs to handle a large throughput of gas while maintaining an appropriate vacuum. A large turbomolecular pump attached to the base of the chamber is used to evacuate the system at a rate of up to 2200 L/s. The cubic design of the chamber allows for ports to be situated at five different anode-to-sample distances (the ports are centered at 40, 50, 130, 210,

and 220 mm from the anode), allowing some control over how long the electron pulse propagates before it interacts with the sample. Having three DN40CF flanges (left, right, and top) at each distance enables the sample to be introduced through the top of the chamber (directly opposite the pump), while other components such as a cold trap and pump laser can be brought in through the side ports. The availability of pairs of opposite ports will also allow grating-enhanced ponderomotive measurements to be performed,⁴⁴ in order to determine the electron-pulse durations at the sample positions.

As a test of the apparatus we recorded diffraction patterns for a polycrystalline sample of platinum mounted on an *xyz* translator at a distance of 115 mm from the anode (introduced through the 130 mm port); the phosphor screen detector was 215 mm beyond the sample. For future gas-phase studies, the sample holder which supports TEM grids perpendicularly to the electron beam will be replaced by a gas-inlet system, while other aspects of the apparatus setup will remain relatively unchanged.

E. Detector

Diffraction images are recorded using a micro-channel plate (MCP) / phosphor screen / charge coupled device (CCD) camera setup. An aluminum beam cup (7.5 millimeters in diameter) is mounted in front of the center of the detector to prevent the unscattered electron beam from hitting the phosphor which could both damage the screen and result in a very bright spot of light that would dominate the diffraction pattern; it also acts as a Faraday cup to measure the current of the electron beam. Electrons scattered by the diffraction sample first encounter a grounded mesh ensuring that they propagate through a field-free region. Immediately after the mesh is the MCP, which has an active area 80 mm in diameter; a potential of up to +2 kV is applied across the MCP. The enhanced diffraction pattern is then imaged on a 115 mm phosphor screen, comprising a 3 mm thick glass plate coated with 50 μm of P22 phosphor and 50 nm of aluminum, allowing for the dissipation of charge. The screen is held in an aluminum mount at a potential of up to +5 kV relative to the grounded mesh, and this is further mounted on a DN160CF flange with a viewport through which a Stingray F-146B CCD records the diffraction patterns. The camera is coupled to a Schneider 17 mm focal-length lens with an $f/0.95$ aperture, allowing the camera to be positioned a few millimeters from the viewport with the whole screen visible; the wide aperture allows the lens to work well in low light conditions.

Image enhancement using the MCP was incorporated into the design because of the very small beam currents used in the TRED experiments. For each electron that impinges on a

pore in the MCP, approximately 10^6 additional electrons are produced to enhance the image.⁴⁵ Without the MCP, we were able to image unscattered electron beams only when there were more than 5,000 electrons per pulse; in this set-up observing a diffraction pattern was difficult even when recording images for a number of hours. With the MCP, it was possible to observe an image of a beam with a current that was below the noise level of the picoammeter used to record the current (estimated to be less than 500 electrons per pulse).

With the detector positioned 215 mm from the sample, it allows for diffraction data to be observed to a maximum of $s = 195 \text{ nm}^{-1}$, for 45 keV electrons, where s is a function of the scattering angle, θ , and the electron wavelength, λ , such that $s = (4\pi \sin \theta) / \lambda$.

IV. CALIBRATION AND RESULTS

A. Number of electrons

The number of electrons per pulse affects both the beam spot size and pulse duration, and these in turn influence both the spatial and temporal resolutions of the apparatus. In order to obtain the desired characteristics (small transverse beam size and short electron pulse duration), it is important to be able to measure and control the number of electrons per pulse. This is achieved by varying the power of the laser reaching the photocathode by adjusting the alignment of the optical axis of the second harmonic generation (SHG) crystal. The laser power is measured using a power meter and the number of electrons determined using a picoammeter to measure the average beam current and dividing by the repetition rate of the laser. With an average laser power of approximately 0.3 W entering the harmonics setup, we can accurately measure between 10^3 and 10^7 electrons per pulse which can be varied depending on whether we required better time resolution or shorter collection times for a given experiment. Figure 3 shows the number of electrons observed per pulse with respect to the angle of the SHG crystal.

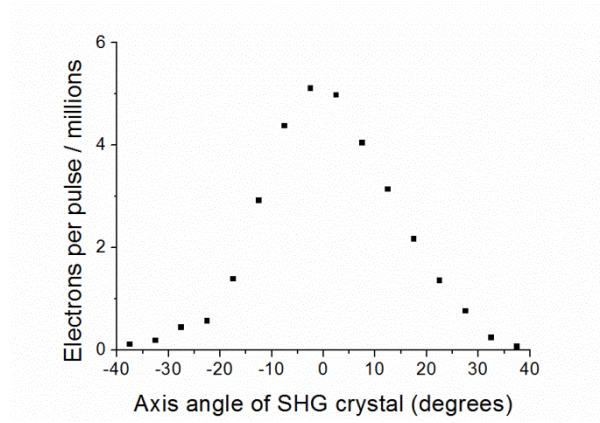


FIG. 3. The number of 45 keV electrons passing through a 1 mm diameter aperture in the anode, with respect to the axis angle of the second harmonic generation crystal.

B. Beam size and magnetic lens

In order to achieve good spatial resolution we require the electron beam spot size to be small at the sample and at the detector. To help achieve this, the magnetic lens discussed in Section III.C is used to focus the beam. To quantitatively demonstrate the focusing properties of the magnetic lens on the electron beam width, a beam containing approximately 10^4 electrons per pulse was directed towards a $500\ \mu\text{m}$ aperture at the sample position. The aperture blocks part of the beam and those electrons that do pass through hit the Faraday cup where the current is measured. By scanning the position of the aperture across the beam and recording how the current varies, two-dimensional profiles of the beam in the x and y directions are obtained [see Figure 4(a)].

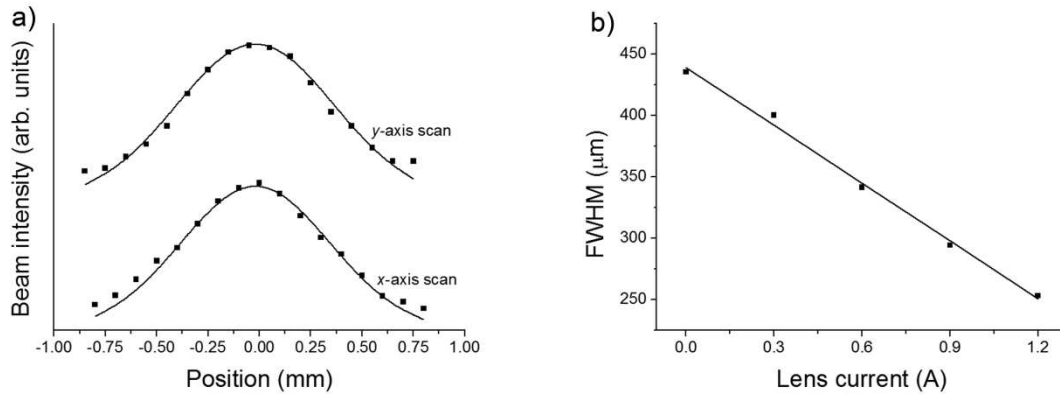


FIG. 4. a) The perpendicular transverse beam widths (x and y) at the sample position, for a 45 keV electron beam containing approximately 10^4 electrons per pulse (average FWHM size of $435\ \mu\text{m}$, maximum intensity measured as 650 fA). b) The average FWHM beam size at the sample position as a function of magnetic lens current.

The measurements show the electron beam to be Gaussian in shape, with the FWHM beam size reducing linearly as the lens current is increased, as shown in Figure 4(b).

Extensive simulations (to be published separately)⁴¹ have also shown that, for certain lens currents, the beam will remain well collimated as it travels to the detector, with only a small increase in pulse duration predicted.

C. Diffraction

While this instrument was developed as a time-resolved gas-phase diffractometer, the first study performed was for a polycrystalline sample of platinum; the well-defined, predictable, closely-spaced rings produced by a polycrystalline sample allow for the instrument to be easily calibrated without the added complexities of introducing a gaseous sample. A 20 nm thick layer of Pt was deposited onto a carbon-coated TEM grid, mounted on an *xyz* manipulator, and positioned in the electron beam. Images were recorded with potentials of +1.9 kV applied to the MCP, and +4.1 kV applied to the phosphor screen. Individual images were stacked before background images, recorded under identical conditions but without the sample present, were subtracted from the sample data. By doing this we remove any background electron scattering, reflected light, or systematic errors which would distort the data. For comparison of the effectiveness of our magnetic lens, diffraction patterns for the Pt sample were recorded both with the magnetic lens off and on. The scattering intensities of the observed diffraction rings for both sets of data were extracted by radially averaging around the center of the pattern using custom-written MATLAB code. The intensity curves obtained from both experiments are shown in Figure 5(a). One can clearly see that the resolution of the experiment has improved with the introduction of the magnetic lens, as the peaks become more defined, compared to the broader, overlapping, and, in some cases, barely discernible features recorded without the magnetic lens.

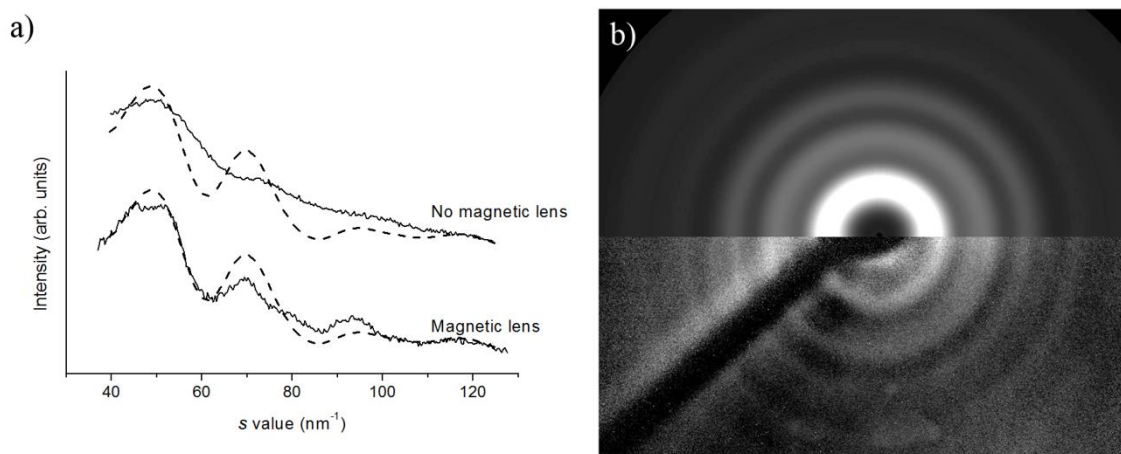


FIG. 5. a) Comparison of diffraction intensities from experiments with the magnetic lens off (top), and on (bottom); the curves are offset for clarity. Theoretical scattering curves showing

what is predicted for a well-focused electron beam are shown as a dashed line. b) Comparison of theoretical diffraction pattern (top) and experimental diffraction pattern (bottom) collected using the magnetic lens.

The extracted diffraction data have also been compared to a theoretical scattering intensity curve, shown as dashed lines in Figure 5(a), based on the expected face-centered cubic polycrystalline diffraction pattern for platinum, with peak widths based on the best electron beam width we hope to have at the detector. One can clearly see that the positions of the peaks in the theoretical and experimental data match when data are collected with the magnetic lens on. We have shown the same theoretical curve on top of the data extracted from diffraction patterns recorded without the magnetic lens, highlighting the lack of resolution when the lens is omitted. From the data it is possible to calculate the resolution of the experiment as $\Delta s = 6.7 \text{ nm}^{-1}$ with the magnetic lens present. Using the predicted scattering curve it was also possible to create a theoretical diffraction pattern. This is overlaid on the experimental diffraction pattern in Figure 5(b), again emphasizing the match between experimental and theory.

V. SUMMARY AND CONCLUSIONS

We have designed, built, and tested an electron diffractometer that uses a compact electron gun to produce pulses of electrons predicted to have a duration of approximately 375 fs, and with a potential experimental time resolution of approximately 670 fs at 100 kV, for experiments that do not use tilted laser wavefronts.⁴⁶ We have demonstrated that this pulsed electron gun can yield diffraction patterns for a polycrystalline sample of platinum in a timely manner, and that the spatial resolution of the experiment can be enhanced with the use of a magnetic lens. Our focus now moves to performing static gas-phase studies, before collecting time-resolved data for photoinduced dynamic systems in the near future.

ACKNOWLEDGMENTS

The authors are grateful to the EPSRC for funding (EP/I004122), while M.S.R. thanks the University of Edinburgh Moray Fund for funding a project to build the magnetic lens, and P.D.L. thanks the University of Edinburgh Innovation Initiative Fund for software provision. We acknowledge Prof. Eleanor Campbell of the University of Edinburgh for allowing access to the laser laboratory in Edinburgh, and the U.K. Laser Loan Pool for the loan of UFL2 (project 13250016). We thank Stuart Young (University of York), Dr. J. Olof Johansson (University of Edinburgh), and Prof. Dwayne Miller and Dr. Stuart Hayes (both MPSD Hamburg) for useful discussions. Dr. Oleg Nerushev and Dave Coulthard were generous in

their assistance in producing photocathodes, Dr. Konstantin Kamenev assisted in the winding of the magnetic lens, and Prof. Jun Yuan helped to prepare the platinum samples. We are grateful to David Paden, Chris Mortimer, Chris Rhodes, Jon Hamstead, and Wayne Robinson for building numerous mechanical and electronic components for the apparatus.

- ¹ C. Davisson, and L. H. Germer, *Nature* **119**, 558 (1927).
- ² T. S. Rose, M. J. Rosker, and A. H. Zewail, *J. Chem. Phys.* **88**, 6672 (1988).
- ³ G. Sciaini, and R. J. D. Miller, *Rep. Prog. Phys.* **74**, 096101 (2011).
- ⁴ M. Gao, C. Lu, H. Jean-Ruel, L. C. Liu, A. Marx, K. Onda, S. Koshihara, Y. Nakano, X. Shao, T. Hiramatsu, G. Saito, H. Yamochi, R. R. Cooney, G. Moriena, G. Sciaini, and R. J. D. Miller, *Nature* **496**, 343 (2013).
- ⁵ A. A. Ischenko, V. V. Golubkov, V. P. Spiridonov, A. V. Zgurskii, A. S. Akmanov, M. G. Vabischevich, and V. N. Bagratashvili, *Appl. Phys. Lett. B: Lasers Opt.* **32**, 161 (1983).
- ⁶ J. D. Ewbank, W. L. Faust, J. Y. Luo, J. T. English, D. L. Monts, D. W. Paul, Q. Dou, and L. Schäfer, *Rev. Sci. Instrum.* **63**, 3352 (1992).
- ⁷ J. C. Williamson, and A. H. Zewail, *Proc. Natl. Acad. Sci. USA* **88**, 5021 (1991).
- ⁸ J. C. Williamson, M. Dantus, S. B. Kim, and A. H. Zewail, *Chem. Phys. Lett.* **196**, 529 (1992).
- ⁹ J. C. Williamson, J. Cao, H. Ihee, H. Frey, and A. H. Zewail, *Nature* **386**, 159 (1997).
- ¹⁰ H. Ihee, V. A. Lobastov, U. M. Gomez, B. M. Goodson, R. Srinivasan, C.-Y. Ruan, and A. H. Zewail, *Science* **291**, 458 (2001).
- ¹¹ J. C. Williamson, and A. H. Zewail, *Chem. Phys. Lett.* **209**, 10 (1993).
- ¹² B.-L. Qian, and H. E. Elsayed-Ali, *J. Appl. Phys.* **91**, 462 (2002).
- ¹³ B.-L. Qian, and H. E. Elsayed-Ali, *J. Appl. Phys.* **92**, 1643 (2002).
- ¹⁴ B. J. Siwick, J. R. Dwyer, R. E. Jordan, and R. J. D. Miller, *J. Appl. Phys.* **92**, 1643 (2002).
- ¹⁵ B. J. Siwick, J. R. Dwyer, R. E. Jordan, and R. J. D. Miller, *J. Appl. Phys.* **94**, 807 (2003).
- ¹⁶ T. van Oudheusden, P. L. E. M. Pasmans, S. B. van der Geer, M. J. de Loos, M. J. van der Wiel, and O. J. Luiten, *Phys. Rev. Lett.* **105**, 264801 (2010).
- ¹⁷ M. Gao, H. Jean-Ruel, R. R. Cooney, J. Stampe, M. De Jong, M. Harb, G. Sciaini, G. Moriena, and R. J. D. Miller, *Opt. Exp.* **20**, 12048 (2012).
- ¹⁸ R. P. Chatelain, V. R. Morrison, C. Godbout, and B. J. Siwick, *Appl. Phys. Lett.* **101**, 081901 (2012).

- ¹⁹ J. D. Geiser, and P. Weber in *Time-Resolved Electron and X-ray Diffraction* (SPIE: San Diego, vol. 2521, 1995).
- ²⁰ P. Baum, Chem. Phys. **423**, 55 (2013).
- ²¹ J. B. Hastings F. M. Rudakov, D. H. Dowell, J. F. Schmerge, J. D. Cardoza, J. M. Castro, S. M. Gierman, H. Loos, and P. M. Weber, Appl. Phys. Lett. **89**, 184109 (2006).
- ²² R. Li, W. Huang, Y. Du, J. Shi, J. Hua, H. Chen, T. Du, H. Xu, and C. Tang, Rev. Sci. Instrum. **81**, 036110 (2010).
- ²³ P. Musumeci, J. T. Moody, C. M. Scoby, M. S. Gutierrez, and M. Westfall, Appl. Phys. Lett. **97**, 063502 (2010).
- ²⁴ B. J. Siwick, J. R. Dwyer, R. E. Jordan, and R. J. D. Miller, Science **302**, 1382 (2003).
- ²⁵ B. J. Siwick, J. R. Dwyer, R. E. Jordan, and R. J. D. Miller, Chem. Phys. **299**, 285 (2004).
- ²⁶ R. C. Dudek, and P. M. Weber, J. Phys. Chem. A **105**, 4167 (2001).
- ²⁷ M. Harb, R. Ernstorfer, C. T. Hebeisen, G. Sciaini, W. Peng, T. Dartigalongue, M. A. Eriksson, M. G. Lagally, S. G. Kruglik, and R. J. D. Miller, Phys. Rev. Lett. **100**, 155504 (2008).
- ²⁸ R. K. Raman, Y. Murooka, C.-Y. Ruan, T. Yang, S. Berber, and D. Tománek, Phys. Rev. Lett. **101**, 077401 (2008).
- ²⁹ G. Sciaini, M. Harb, S. G. Kruglik, T. Payer, C. T. Hebeisen, F.-J. Meyer zu Heringdorf, M. Yamaguchi, M. Horn-von Hoegen, R. Ernstorfer, and R. J. D. Miller, Nature **458**, 56 (2009).
- ³⁰ H. Jean-Ruel, M. Gao, M. A. Kochman, C. Lu, C. Liu, R. R. Cooney, C. A. Morrison, and R. J. D. Miller, J. Phys. Chem. B. **117**, 15894 (2013).
- ³¹ A. Janzen, B. Krenzer, P. Zhou, D. Von der Linde, and M. Horn-von Hoegen, Surf. Sci. **600**, 4094 (2006).
- ³² A. Hanisch-Blicharski, A. Janzen, B. Krenzer, S. Wall, F. Klasing, A. Kalus, T. Frigge, M. Kammler, and M. Horn-von Hoegen, Ultramicroscopy **127**, 2 (2013).
- ³³ H. Ihee, V. A. Lobastov, U. M. Gomez, B. M. Goodson, R. Srinivasan, C.-Y. Ruan, and A. H. Zewail, Science **291**, 458 (2001).
- ³⁴ C. J. Hensley, J. Yang, and M. Centurion, Phys. Rev. Lett. **109**, 133202 (2012).
- ³⁵ B. J. Siwick, PhD thesis, *Femtosecond Electron Diffraction Studies of Strongly-Driven Structural Phase Changes* (University of Toronto, 2004).
- ³⁶ T. van Oudheusden, E. F. de Jong, S. B. van der Geer, W. P. E. M. Op 't Root, O. J. Luiten, and B. J. Siwick, J. Appl. Phys. **102**, 093501 (2007).

- ³⁷ G. H. Kassier, K. Haupt, N. Erasmus, E. G. Rohwer, H. M. von Bergmann, H. Schwoerer, S. M. M. Coelho, and F. D. Auret, *Rev. Sci. Instrum.* **81**, 105103 (2010).
- ³⁸ M. Eichberger, N. Erasmus, K. Haupt, G. H. Kassier, A. von Flotow, J. Demsar, and H. Schwoerer, *Appl. Phys. Lett.* **102**, 121106 (2013).
- ³⁹ S. B. van der Geer, and M. J. de Loos, *General Particle Tracer*, Elements 1 (2009).
- ⁴⁰ D. A. Dahl, *Int. J. Mass Spectrom.* **200**, 3 (2000).
- ⁴¹ M. S. Robinson, P. D. Lane, and D. A. Wann, manuscript in preparation.
- ⁴² G. Blaise, A. J. Duran, C. Le Gressus, B. G. A. Jüttner, R. Latham, A. Maitland, B. Mazurek, H. C. Miller, H. Padamsee, M. F. Rose, A. M. Shroff, and N. Xu, *High Voltage Vacuum insulation: Basic Concepts and Technological Practice* (Harcourt Brace and Company, 1995).
- ⁴³ See, for example, D. J. Griffiths, *Introduction to electrodynamics* 3rd Edition (Pearson, 1998).
- ⁴⁴ C. T. Hebeisen, R. Ernstorfer, M. Harb, T. Dartigalongue, R. E. Jordan, and R. J. D. Miller, *Opt. Lett.* **31**, 3517 (2006).
- ⁴⁵ R. S. Fender, PhD thesis, *Advances in Gas-Phase Electron Diffraction*, (University of Edinburgh, 1996).
- ⁴⁶ P. Baum, A. H. Zewail, *P. Natl. Acad. Sci. USA* **103**, 16105 (2006).